

## Borderline magnetism in $\text{Sr}_4\text{Ru}_3\text{O}_{10}$ : Impact of La and Ca doping on itinerant ferromagnetism and metamagnetism

S. Chikara, V. Durairaj, W. H. Song,<sup>†</sup> Y. P. Sun,<sup>†</sup> X. N. Lin, A. Douglass, and G. Cao\*  
*Department of Physics and Astronomy, University of Kentucky, Lexington, Kentucky 40506, USA*

P. Schlottmann

*Department of Physics and National High Magnetic Field Laboratory, Florida State University, Tallahassee, Florida 32306, USA*

S. Parkin

*Department of Chemistry, University of Kentucky, Lexington, Kentucky 40506, USA*

(Received 22 January 2006; revised manuscript received 8 May 2006; published 15 June 2006)

An investigation of La and Ca doped  $\text{Sr}_4\text{Ru}_3\text{O}_{10}$ , featuring a coexistence of interlayer ferromagnetism and intralayer metamagnetism, is presented. La doping readily changes magnetism between ferromagnetism and metamagnetism by tuning the density of states. It also results in *different* Curie temperatures for the *c*-axis and the basal plane, highlighting a rare spin-orbit coupling with the crystal field states. In contrast, Ca doping enhances the *c*-axis ferromagnetism and the magnetic anisotropy. La doping also induces a dimensional crossover in the interlayer transport whereas Ca doping exhibits a tunneling magnetoresistance and an extraordinary  $T^{3/2}$  dependence of the resistivity. The drastic changes caused by the doping demonstrate a rare borderline magnetism that is delicately linked to the interplay of the density of states and spin-orbit coupling.

DOI: 10.1103/PhysRevB.73.224420

PACS number(s): 75.47.-m

### I. INTRODUCTION

Understanding itinerant ferromagnetism and metamagnetism is a longstanding challenge in condensed matter physics.<sup>1,2</sup> According to the Stoner model,<sup>3</sup> the condition for spontaneous ferromagnetism requires that the Coulomb exchange interaction,  $U$ , is strong and, in addition, the density of states at the Fermi surface,  $g(E_F)$ , is large, so that  $Ug(E_F) \geq 1$ , which is known as the Stoner criterion. If  $Ug(E_F)$  is large but not sufficiently close to 1 (i.e.,  $Ug(E_F) < 1$ ), enhanced paramagnetism characterized by a large and temperature-dependent magnetic susceptibility is expected. The detailed properties of the Stoner enhanced  $\chi(T)$  are determined by the energy dependence of  $g(E)$  in the vicinity of the Fermi level. Peaks of  $g(E)$  are often related to Van Hove singularities and intimately coupled to magnetism and phonons (lattice deformations). Hence, the field-induced itinerant metamagnetism<sup>2,4-6</sup> observed in several materials such as  $\text{Sr}_3\text{Ru}_2\text{O}_7$  (Refs. 7 and 8),  $\text{Y}(\text{Co}_{1-x}\text{Al}_x)_2$  (Ref. 5) and other Co compounds<sup>6</sup> is believed to be induced by a nearby Stoner instability. Recent studies on correlated metals such as  $\text{MnSi}$ <sup>9</sup> and  $\text{Sr}_3\text{Ru}_2\text{O}_7$  (Refs. 7, 8, and 10) reveal phenomena consistent with quantum criticality due to the onset of itinerant ferromagnetism and the critical end point of a first-order metamagnetic transition, respectively. The essence of this physics has been captured by a simple model<sup>11</sup> invoking a minimum of  $g(E)$  ( $\text{MnSi}$ ) and a two-dimensional Van Hove singularity for the ruthenate. Clearly, itinerant ferromagnetism and metamagnetism sensitively depend on  $U$  and  $g(E_F)$ , and are not expected to coexist. But  $\text{Sr}_4\text{Ru}_3\text{O}_{10}$  under doping defiantly shows the coexistence of both. It is this coexistence that suggests new physics.

$\text{Sr}_4\text{Ru}_3\text{O}_{10}$  belongs to the layered ruthenate series,  $(\text{Ca}, \text{Sr})_{n+1}\text{Ru}_n\text{O}_{3n+1}$  ( $n$ =number of Ru-O layers/unit cell). Rich with novel physical phenomena rarely found in other

materials, these materials share as a central feature the extended  $4d$ -electron orbitals, which lead to comparable and thus competing energies for crystalline fields (CEF), Hund's rule interactions, spin-orbit coupling,  $p$ - $d$  hybridization, and electron-lattice coupling. The deformations and relative orientations of corner-shared  $\text{RuO}_6$  octahedra crucially determine the CEF level splitting and the band structure, and hence the nature of the ground state. As a result, the physical properties are highly dimensionality (or  $n$ ) dependent and susceptible to perturbations such as the application of magnetic fields, pressure, and slight changes in chemical compositions (electron-lattice coupling). These characteristics are illustrated in  $\text{Ca}_{n+1}\text{Ru}_n\text{O}_{3n+1}$  and  $\text{Sr}_{n+1}\text{Ru}_n\text{O}_{3n+1}$  ( $n=1, 2, 3, \infty$ ): The former are on the verge of a metal-insulator transition and prone to antiferromagnetism that changes with  $n$ , whereas the latter are metallic, and evolve from paramagnetism ( $n=1,2$ ) to a ferromagnetic state ( $n=\infty$ ) with increasing  $n$ .<sup>7,8,10,12-31</sup>

Situated between  $n=2$  and  $n=\infty$ , the triple-layered  $\text{Sr}_4\text{Ru}_3\text{O}_{10}$  ( $n=3$ ) displays complex phenomena ranging from tunneling magnetoresistance, low frequency quantum oscillations<sup>25-28</sup> to switching behavior.<sup>29</sup> The most intriguing feature, however, is borderline magnetism: While *along the c axis* (perpendicular to the layers),  $\text{Sr}_4\text{Ru}_3\text{O}_{10}$  shows ferromagnetism [ $Ug(E_F) \geq 1$ ] with a saturation moment  $M_S$  of  $1.13 \mu_B/\text{Ru}$  and a Curie temperature  $T_C$  at 105 K followed by increased spin polarization below  $T_M=50$  K, it features for the field in *the ab plane* a sharp peak in the magnetization at  $T_M=50$  K and a first-order metamagnetic transition,<sup>26</sup> a situation strikingly similar to Stoner enhancement [ $Ug(E_F) < 1$ ] responsible for the enhanced paramagnetism and itinerant metamagnetism.<sup>4-8,11</sup> The coexistence of the interlayer ferromagnetism and the intralayer metamagnetism, i.e., the anisotropy in the field response, is not expected from simple theoretical arguments,<sup>1,2,6</sup> and has then to arise from

the two-dimensional Van Hove singularity (logarithmical divergence) close to the Fermi level<sup>11</sup> in conjunction with the coupling of the spins to the crystalline field orbital states and the lattice.  $\text{Sr}_4\text{Ru}_3\text{O}_{10}$  ( $n=3$ ) is therefore a unique system that is delicately positioned on the borderline separating its closest neighbors, the ferromagnet  $\text{SrRuO}_3$  ( $n=\infty$ )<sup>20</sup> and the paramagnet  $\text{Sr}_3\text{Ru}_2\text{O}_7$  ( $n=2$ ),<sup>7,8</sup> and provides a rare opportunity to study itinerant ferromagnetism and metamagnetism by slightly tuning  $g(E_F)$  through band filling (electron doping) and bandwidth control (structural alteration).

In this paper we report results of our study on  $\text{Sr}_4\text{Ru}_3\text{O}_{10}$  with  $\text{Sr}^{2+}$  being replaced by small amounts of  $\text{La}^{3+}$  and  $\text{Ca}^{2+}$  ions. Probing magnetism with these substitutions offers the following advantages: A concentration  $x$  of  $\text{La}^{3+}$  dopes the system with  $x$  electrons on the Ru sites, altering  $g(E_F)$  and the exchange splitting  $\Delta$ . In addition, the  $\text{La}^{3+}$  and  $\text{Ca}^{2+}$  ions are significantly smaller than the  $\text{Sr}^{2+}$  ion (the ionic radii:  $r_{\text{La}}=1.03 \text{ \AA}$  and  $r_{\text{Ca}}=1.00 \text{ \AA}$ , compared to  $r_{\text{Sr}}=1.18 \text{ \AA}$ ); hence, low concentration doping enhances the buckling of the  $\text{RuO}_6$  octahedra, varying the exchange interaction or bandwidth while preserving the crystal structure. Because of the similarity of the ionic size, the impact of the La and Ca doping on the structural distortions is expected to be similar. Therefore, studying and comparing responses to La and Ca doping not only reveals different phenomena, but also differentiates the effect of electron doping and the structural distortion on the itinerant magnetism. Indeed, properties of  $(\text{Sr}_{1-x}\text{La}_x)_4\text{Ru}_3\text{O}_{10}$  and  $(\text{Sr}_{1-x}\text{Ca}_x)_4\text{Ru}_3\text{O}_{10}$  with  $0 \leq x \leq 0.13$  (Ref. 32) vary widely and drastically. Most significantly, La doping effectively reduces  $g(E_F)$ ,  $\Delta$  and  $M_S$ , leading to an evolution from ferromagnetism to metamagnetism along the  $c$  axis but a reverse development within the basal plane. It also results in *different* Curie temperatures for the  $c$  axis and the basal plane that bring to light an unusual interplay of the spin-orbit coupling with the CEF states. In sharp contrast, Ca doping enhances the  $c$  axis spontaneous ferromagnetism, but drastically weakens the basal plane magnetization. In terms of transport properties, La doping induces a dimensional crossover in the interlayer transport at high temperatures and Ca doping results in a large tunneling magnetoresistance at  $x=0.02$  and an unusual  $T^{3/2}$ -power law for the resistivity at  $x=0.13$  below  $T_C$ , suggesting non-Fermi-liquid behavior.<sup>9</sup> The large array of phenomena presented illustrates the rare borderline magnetism that is critically determined by the interplay of the density of the states and spin-orbit coupling with the crystal field states of the  $\text{RuO}_6$ -octahedra.

## II. RESULTS AND DISCUSSION

Figure 1 displays the changes of the lattice parameters  $a$  and  $c$  axis as a function of  $x$ . The structure of  $\text{Sr}_4\text{Ru}_3\text{O}_{10}$  is slightly orthorhombic with the room-temperature (RT) lattice parameters  $a=5.4982 \text{ \AA}$ ,  $b=5.4995 \text{ \AA}$ , and  $c=28.5956 \text{ \AA}$  and a space group of  $Pb3m$  (the lattice parameter  $b$  axis, which is only slightly longer than the  $a$  axis and behaves similarly, is not shown). Both La and Ca doping causes no structural changes but the lattice parameters vary with La and Ca doping in a few interesting ways. As shown in Fig. 1(a), the  $c$  axis expectedly shortens with increasing  $x$  with Ca

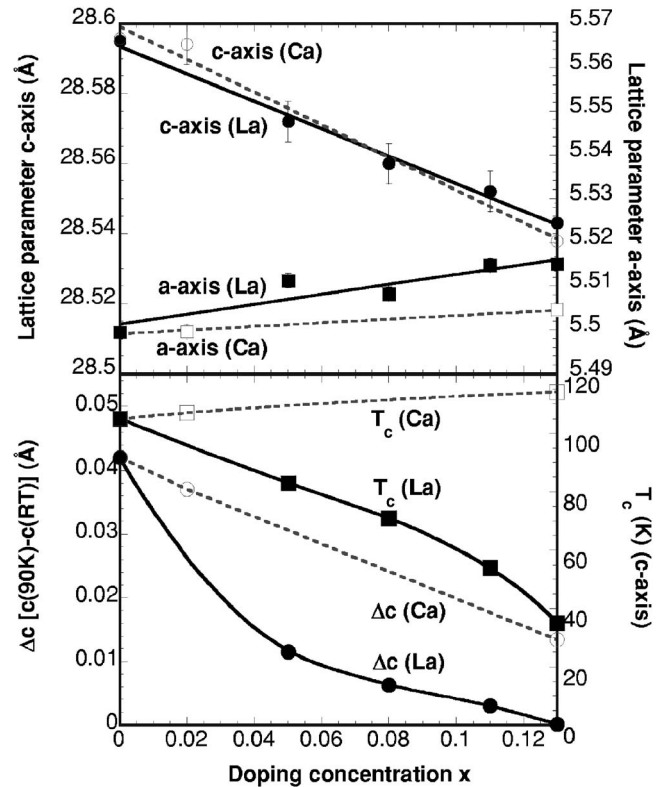


FIG. 1. The doping concentration  $x$  dependence of (a) lattice parameters  $a$  and  $c$  axis, and (b)  $\Delta c$  defined as  $[c(90 \text{ K})-c(\text{RT})]$  and  $c$ -axis Curie temperature  $T_c$  (right scale) for La doping (solid symbols and solid lines) and Ca doping (empty symbols and dashed lines).

doping showing a stronger effect. But the  $a$  axis grows with increasing  $x$ , and this growth is quite stronger for La doping, which causes a slight increase in the volume of the unit cell. This increase may be in part associated with the additional electron added from the trivalent  $\text{La}^{3+}$ . A remarkable structural feature of  $\text{Sr}_4\text{Ru}_3\text{O}_{10}$  is that the  $c$  axis grows with *decreasing* temperature.<sup>25,26</sup> As  $x$  increases, the  $c$  axis change with temperature becomes smaller as shown in Fig. 1(b) where  $\Delta c$  defined as  $c(90 \text{ K})-c(\text{RT})$  vs  $x$  is plotted. It is rather noticeable that the La doping rapidly reduces  $\Delta c$  that becomes almost zero at  $x=0.13$ . In contrast, the Ca doping shows a smaller impact on  $\Delta c$  which is still significant at  $x=0.13$ . It is interesting that the  $c$  axis  $T_c$  appears to be somewhat associated with  $\Delta c$ , particularly,  $T_c$  for La doping decreases with vanishing  $\Delta c$ , suggesting a significant magnetoelastic effect in the systems.

Figure 2 shows the temperature dependence of magnetization  $M$  for  $(\text{Sr}_{1-x}\text{La}_x)_4\text{Ru}_3\text{O}_{10}$  for (a) the  $c$  axis and (b) the  $ab$  plane, and for  $(\text{Sr}_{1-x}\text{Ca}_x)_4\text{Ru}_3\text{O}_{10}$  for (c) the  $c$  axis and (d) the  $ab$  plane. This figure contrasts the impact of the La and Ca doping on  $M(T)$ . As seen in Fig. 2(a), the magnetization along the  $c$  axis,  $M_c$ , displays a gradual evolution from the ferromagnetism to paramagnetism with increasing  $x$ , as manifested by the rapid decrease of  $T_c$ , indicated by the vertical arrows. Upon cooling the transition at  $T_M$  (denoted with arrowheads), which for  $x=0$  marks the increase in  $M_c$  at 50 K, develops into a sharp downturn for  $x=0.05, 0.08$ , and

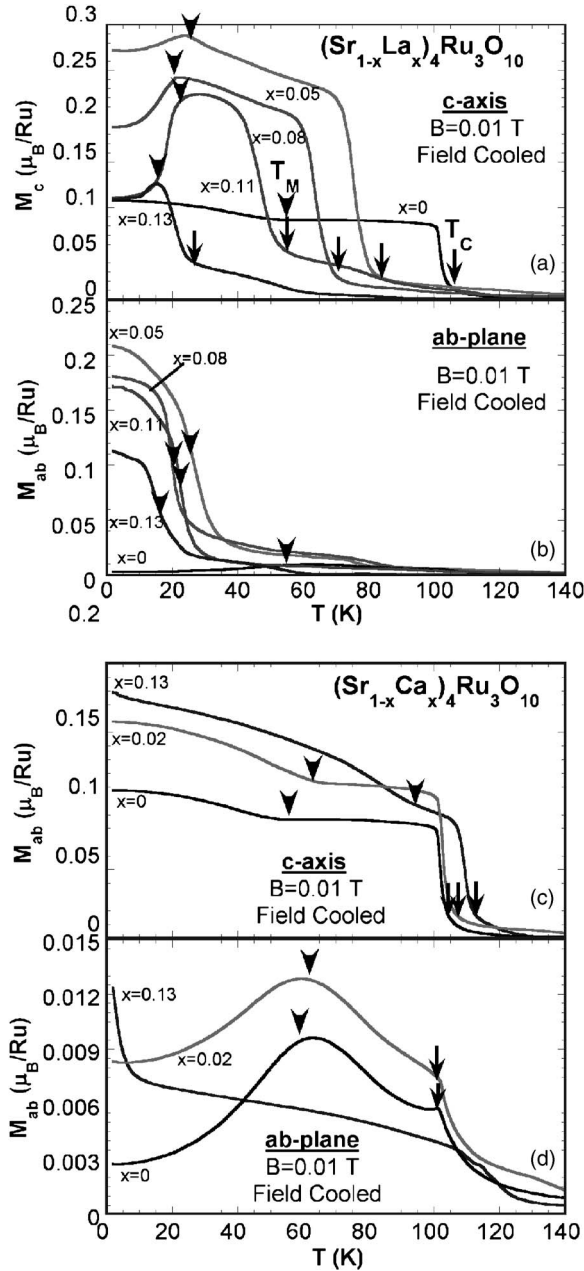


FIG. 2. The magnetization as a function of temperature at  $B=0.01$  T for  $(\text{Sr}_{1-x}\text{La}_x)_4\text{Ru}_3\text{O}_{10}$  for the field (a) along the  $c$  axis and (b) in the  $ab$  plane, and for  $(\text{Sr}_{1-x}\text{Ca}_x)_4\text{Ru}_3\text{O}_{10}$  (c) along the  $c$  axis and (d) in the  $ab$  plane. Note that  $c$ -axis  $T_C$  is indicated by arrows whereas  $c$ -axis  $T_M$  and  $ab$ -plane  $T_C$  are indicated by arrowheads and that  $c$ -axis  $T_C$  in (a) corresponds to no clear anomalies in the  $ab$  plane in (b).

0.11, and eventually into a peak at  $x=0.13$ , signaling the entry into the paramagnetic state. In contrast, within the  $ab$  plane ferromagnetism occurs upon La doping at  $T_M$  where  $M_c$  has its maximum [Fig. 2(b)]. In Fig. 2(b) the arrowheads indicate the emergence of fully developed ferromagnetism. It is striking that  $M_{ab}$  shows only an anomaly at  $T_C$  that is dramatically weaker than that in  $M_c$  [compare Figs. 1(a) and 1(b)]. Evidently, the La doping causes a strong anisotropy in  $M$  favoring ferromagnetism along the  $c$  axis for

$T_M < T < T_C$ . On the other hand, Ca doping preserves the temperature dependence of  $M_c$  and visibly increases  $T_C$  and  $T_M$ , as well as for  $M_{ab}$  for sufficiently small  $x$ , but entirely changes  $M_{ab}$  for  $x=0.13$  [Figs. 2(c) and 2(d)]. The arrows and arrowheads highlight the key features of the temperature dependence of  $M$ . Magnetic anisotropy is frequently observed in ferromagnets, but the spectacular difference in the temperature dependence shown in Fig. 2 further emphasizes the two-dimensional Van Hove singularity close to the Fermi level<sup>11</sup> in conjunction with the coupling of the spins to the crystalline field orbital states and the lattice.

Figure 3 shows the isothermal magnetization  $M(B)$  at  $T=2$  K for  $(\text{Sr}_{1-x}\text{La}_x)_4\text{Ru}_3\text{O}_{10}$  for (a) the  $c$  axis and (b) the  $ab$  plane, and for  $(\text{Sr}_{1-x}\text{Ca}_x)_4\text{Ru}_3\text{O}_{10}$  for (c) the  $c$  axis and (d) the  $ab$  plane. For  $x=0$ , the  $M_c(B)$  is readily saturated with increasing  $B$  at 0.2 T, yielding a  $M_S$  of  $1.13 \mu_B/\text{Ru}$ , i.e., more than a half of the  $2 \mu_B/\text{Ru}$  expected for an  $S=1$  system and comparable to that of  $\text{SrRuO}_3$  (Ref. 20). Metamagnetic behavior develops with increasing  $x$  and becomes well-defined in  $M_c(B)$  for  $x \geq 0.08$  as seen in Fig. 3(a). This is consistent with the enhanced paramagnetism for  $T < T_M$  in  $M_c(T)$  shown in Fig. 2(a). On the other hand,  $M_{ab}(B)$  shows a first-order metamagnetic transition at  $B_c$  ( $=2.5$  T at 2 K) for  $x=0$ . This metamagnetic transition essentially disappears for  $x > 0.05$ , where  $M_{ab}(T)$  shows ferromagnetic behavior [Fig. 2(b)]. The impact of Ca doping is different, since the ferromagnetism  $M_c(B)$  strengthens [Fig. 2(c)], but  $M_{ab}(B)$  shows a higher  $B_c$  ( $=3.5$  T at 2 K) for  $x=0.02$ . The metamagnetism in the  $ab$  plane then disappears at  $x=0.13$  and is replaced by a nearly linear field dependence as shown in Fig. 3(d), indicative of the vanishing ferromagnetism in the basal plane. Figures 4(a) and 4(b) highlight the major impacts of La and Ca doping and their differences: the La doping effectively reduces  $T_C$ ,  $T_M$  (dashed lines), and  $M_S$  (solid lines). However, the Ca doping enhances ferromagnetism along the  $c$  axis, but weakens  $M_{ab}$ . The arrows representing the spins in the three layers schematically describe the effects of the La and Ca doping on the spin configuration. It deserves mentioning that the observed critical field of the metamagnetic transition decreases with increasing temperature in  $x=0$  (Ref. 26) and the La and Ca doped compounds. This behavior is similar to that seen in the metamagnet  $\text{Sr}_3\text{Ru}_2\text{O}_7$  (Ref. 7) and is in good agreement with the theoretical model based on the mean field theory that concludes that the metamagnetism in the layered ruthenates is a result of the Van Hove singularity.<sup>11</sup> The temperature dependence of the metamagnetic state in the ruthenates (e.g.,  $\text{Sr}_3\text{Ru}_2\text{O}_7$  [Ref. 7],  $\text{Ca}_3\text{Ru}_2\text{O}_7$  [Refs. 13 and 17]) is pointedly opposite to that observed in many systems such as the Co based compounds<sup>5</sup> and the theoretical prediction using the Landau-Ginzburg theory that suggests the temperature dependence of the critical field follows a term proportional to  $T^2$  (Ref. 6). Such a difference further highlights the complexity of the itinerant metamagnetism.

However, it cannot be ruled out that the transition could be associated with a first-order magnetization process for a hard direction of a uniaxial system. Particularly, the behavior of  $M_{ab}$  for La doping could be indicative of either uncompensated low-temperature antiferromagnetism or even a non-

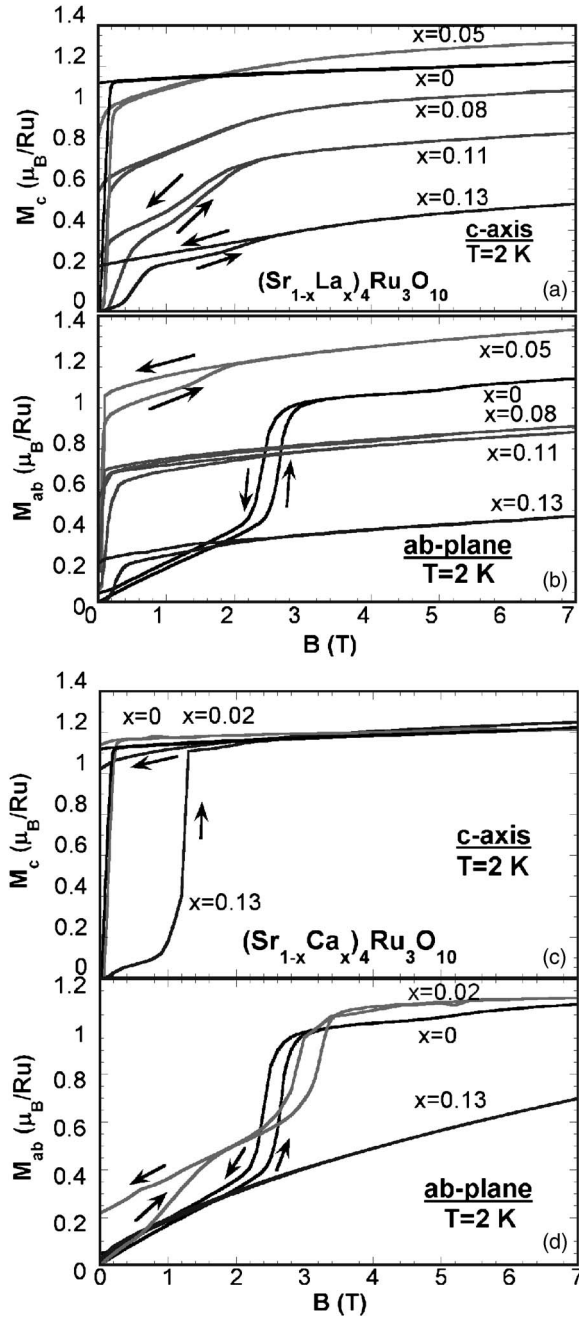


FIG. 3. The isothermal magnetization  $M$  at  $T=2$  K for  $(\text{Sr}_{1-x}\text{La}_x)_4\text{Ru}_3\text{O}_{10}$  for the field (a) along the  $c$  axis and (b) in the  $ab$  plane, and for  $(\text{Sr}_{1-x}\text{Ca}_x)_4\text{Ru}_3\text{O}_{10}$  for (c) along the  $c$  axis and (d) in the  $ab$  plane.

collinear ferromagnetic ordering. In this sense the anomaly at  $T_M$  may be attributed to a spin-reorientation transition. Such a transition may stimulate a first order magnetization process.

Shown in Fig. 5 is the temperature dependence of resistivity,  $\rho$ , at  $B=0$  for  $(\text{Sr}_{1-x}\text{La}_x)_4\text{Ru}_3\text{O}_{10}$  for (a) the  $c$  axis and (b) the basal plane, and for  $(\text{Sr}_{1-x}\text{Ca}_x)_4\text{Ru}_3\text{O}_{10}$  for (c) the  $c$  axis and (d) the basal plane. For  $x=0$ , the  $c$  axis resistivity,  $\rho_c$ , exhibits anomalies corresponding to  $T_C$  and  $T_M$ , and precipitously drops by an order of magnitude from  $T_M(=50$  K)

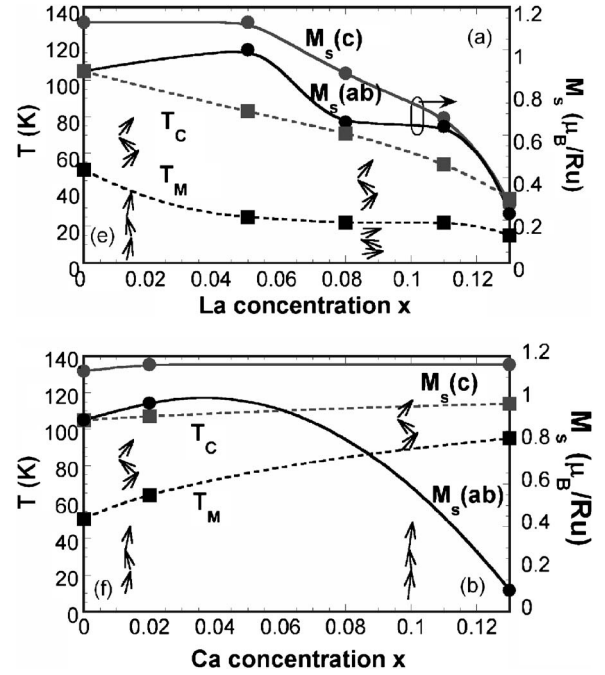


FIG. 4. Dependence of  $T_C$ ,  $T_M$  (dashed lines)  $M_S$  (solid lines) on  $x$  for (a) La doping and (b) Ca doping. The arrows indicate spins in the triple layers and schematically describe the effects of La and Ca doping on the spin configuration.

to 2 K due to the reduction of spin scattering as the spins become strongly polarized below  $T_M$ .<sup>26</sup> This drop in  $\rho_c$  at low  $T$  disappears upon La doping as a result of the strong reduction of spin polarization below  $T_M$  [see Fig. 3(a)]. The increase in residual resistivity  $\rho_0$  can be attributed to an enhancement of the elastic scattering rate  $\tau^{-1}$  either due to increased spin-flip scattering and/or to disorder caused by the doping. In either case the contributions to  $\tau^{-1}$  are essentially temperature-independent. Remarkably, for  $T > T_M$   $\rho_c$  decreases by as much as a factor of 2 with  $x$ , but, on the other hand,  $\rho_{ab}$  increases significantly with  $x$ . This behavior suggests enhanced interlayer hopping but weakened intralayer transport due to doping. It is likely that the La and Ca impurities break the symmetry and give rise to a stronger overlap of the  $d_{xz}$  and  $d_{yz}$  orbitals and hence to a larger conductivity along the  $c$  axis but a reduced one in the  $ab$  plane due to scattering. In addition, a dimensional crossover is facilitated by substituting the smaller ions that shorten the separation between the two-dimensional layers, a situation possibly similar to the temperature-driven crossover in the interlayer transport in layered materials such as  $\text{NaCo}_2\text{O}_4$  and  $\text{Sr}_2\text{RuO}_4$  (Ref. 33).

The temperature-dependence of  $\rho_c$  can be associated with changes in the quasiparticle effective mass  $m_{\text{eff}}$ . With the exception of  $x=0.05$ , the Fermi liquid behavior survives up to  $T < 17$  K for the La doped samples as both  $\rho_c$  and  $\rho_{ab}$  follow the dependence  $\rho = \rho_0 + AT^2$ , where  $A \sim m_{\text{eff}}^2$ . For  $x=0$ ,  $A_c = 1.04 \times 10^{-5} \text{ } \Omega \text{ cm/K}^2$ , and  $A_{ab} = 3.4 \times 10^{-7} \text{ } \Omega \text{ cm/K}^2$ , i.e., the  $A_c/A_{ab}(=31)$  ratio is unusually large, suggesting a strongly anisotropic Fermi surface

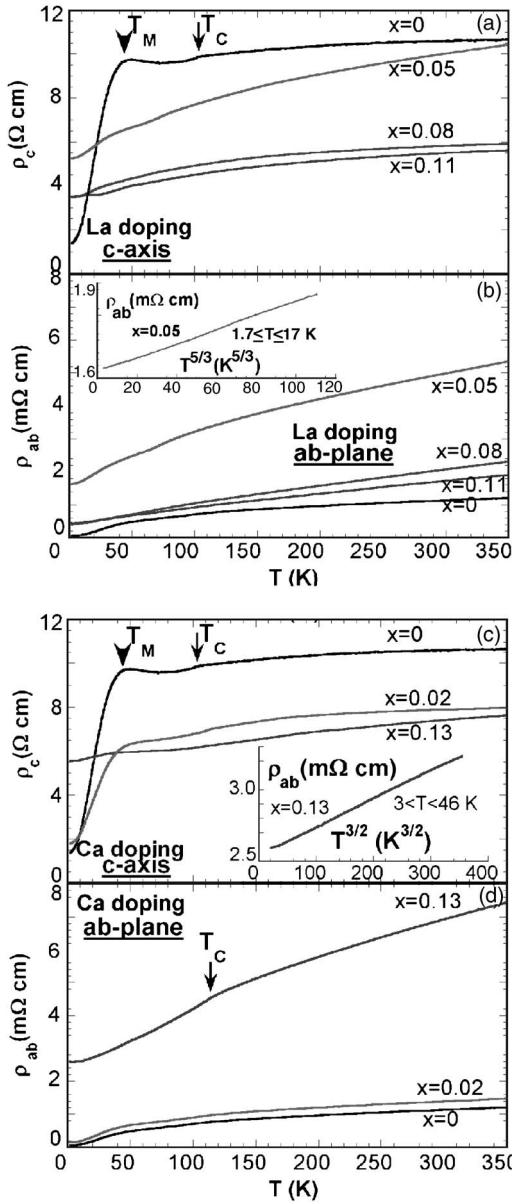


FIG. 5. The resistivity,  $\rho$ , as a function of temperature for  $(\text{Sr}_{1-x}\text{La}_x)_4\text{Ru}_3\text{O}_{10}$  for the field (a) along the  $c$  axis and (b) in the basal plane, and for  $(\text{Sr}_{1-x}\text{Ca}_x)_4\text{Ru}_3\text{O}_{10}$  for (c) along the  $c$  axis and (d) in the basal plane. Inset in panel (b):  $\rho_{ab}$  vs  $T^{5/3}$  for La doping at  $x=0.05$ . Inset in panel (c):  $\rho_{ab}$  vs  $T^{3/2}$  for  $x=0.13$  Ca doping.

or  $m_{\text{eff}}$ .  $A_c/A_{\text{ab}}$  is drastically reduced to 3.9 for  $x=0.08$  and 1.4 for  $x=0.11$  of La doping. This decrease is primarily due to the drop in  $A_c (=2.5 \times 10^{-7} \Omega \text{ cm}/\text{K}^2$  for  $x=0.11$ ) because  $A_{\text{ab}} (=1.8 \times 10^{-7} \Omega \text{ cm}/\text{K}^2$  for  $x=0.11$ ) is only slightly smaller. The smaller  $A_c$  implies a smaller  $m_{\text{eff}}$ , therefore larger electron mobility for the interlayer transport.

It needs to be pointed out that the Fermi-liquid behavior is conspicuously violated for  $x=0.05$  of La doping and  $x=0.13$  of Ca doping. First,  $\rho_{\text{ab}}$  for  $x=0.05$  La doping is exceptionally larger than that for other  $x$ . Second, both  $\rho_{\text{ab}}$  and  $\rho_c$  below 17 K obey a  $T^{5/3}$ -power law as shown (for  $\rho_{\text{ab}}$ ) in the inset in Fig. 5(b). Marginal Fermi-liquid models<sup>1,34</sup>

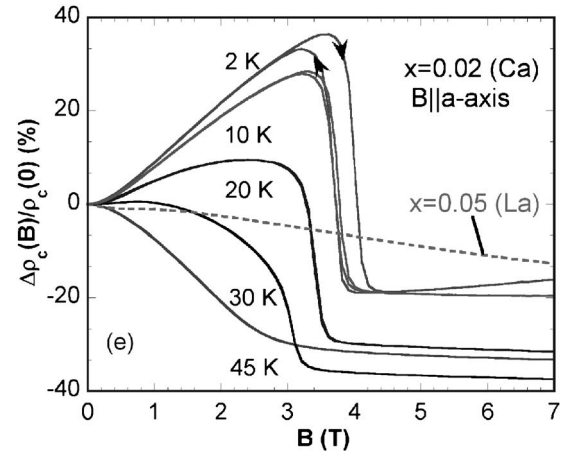


FIG. 6. Magneto-resistivity ratio  $\Delta\rho/\rho(0)$  for Ca doping at  $x=0.02$  as a function of  $B$  applied within the basal plane.

predict power laws of the resistivity as a function of  $T$  with noninteger and even nonuniversal exponents at low  $T$ . The  $T^{5/3}$  power law is anticipated<sup>1</sup> when small angle electron scattering dominates the electronic transport, but is rarely observed in a ferromagnetic state far below  $T_C$ . This  $T^{5/3}$  behavior is intrinsic and unlikely to be due to disorder because the Fermi-liquid behavior is recovered when  $x$  increases as discussed above. More surprisingly, for Ca doping, both  $\rho_{\text{ab}}$  and  $\rho_c$  for  $x=0.13$  show a  $T^{3/2}$  dependence for  $3 < T < 46$  K [see the inset in Fig. 4(c)]. The  $T^{3/2}$  power law, which remains when  $B$  is applied, marks the breakdown of the Fermi-liquid properties. Such behavior, which is also observed in other itinerant ferromagnets such as MnSi at high pressure, is believed to be associated with the effects of diffusive motion of the electrons caused by the interactions between the itinerant electrons and critically damped magnons.<sup>9</sup>

Shown in Fig. 6 is the magneto-resistivity ratio,  $\Delta\rho_c(B)/\rho_c(0)$  with  $\Delta\rho_c(B) = \rho_c(B) - \rho_c(0)$ , for Ca doping at  $x=0.02$  as a function of  $B$  applied within the basal plane. It features a sharp drop at  $B_c$  and reaches a value as large as 40% in the vicinity of and below  $T_M$ . The large reduction in  $\rho_c$  for  $B_{\parallel\text{ab}} > B_c$  implies large ferromagnetic fluctuations in a state without ferromagnetic long-range order immediately above the transition. In contrast,  $\rho_c$  for  $x=0.05$  La doping shows much smaller  $\Delta\rho_c(B)/\rho_c(0)$ , suggesting that scattering is much less spin-dependent as a result of the electron doping.

### III. CONCLUSIONS

This work illustrates that the rare borderline magnetism in  $\text{Sr}_4\text{Ru}_3\text{O}_{10}$  is highly sensitive to  $g(E_F)$  that is critically linked to band filling and structural distortions and that metamagnetism is an immediate neighbor of ferromagnetism. The results indicate that the magnetism determined by  $g(E_F)$  in  $\text{Sr}_4\text{Ru}_3\text{O}_{10}$  seems to be more susceptible to band filling than to a structural distortion. The different  $T_C$  for the  $c$  axis and the basal plane underscore a rare spin-orbit coupling with the crystal field states of the octahedra  $\text{RuO}_6$ . On the other hand,

the structural distortion caused by Ca doping enhances the  $c$  axis ferromagnetism but weakens the basal plane magnetism, causing larger magnetic anisotropy. While the transport is intimately coupled to the magnetism, the largely reduced  $\rho_c$  for  $T > T_M$  signifies a strengthened overlap of  $d_{xz}/d_{yz}$  orbitals and a dimensional crossover. The  $T^{3/2}$  dependence of the resistivity provides evidence for a breakdown of the Fermi liquid model. All unusual behavior clearly results from the

borderline magnetism that calls for new paradigms for studying the itinerant magnetism.

#### ACKNOWLEDGMENTS

This work was supported by NSF Grants Nos. DMR-0240813, DMR-0552267, and DOE Grant No. DE-FG02-98ER45707.

\*Corresponding author. Electronic address: cao@uky.edu

†Present address: Institute of Solid State Physics, Chinese Academy of Sciences, Hefei 230031, Anhui, People's Republic of China.

<sup>1</sup>T. Moriya, *Spin Fluctuations in Itinerant Electron Magnetism* (Springer-Verlag, Berlin, 1985).

<sup>2</sup>Patrik Fazekas, *Lecture Notes on Electron Correlation and Magnetism* (World Scientific, London, 1999).

<sup>3</sup>E. C. Stoner, Proc. R. Soc. London, Ser. A **165**, 372 (1938).

<sup>4</sup>E. P. Wohlfarth and P. Rhodes, Philos. Mag. **7**, 1817 (1962).

<sup>5</sup>T. Sakakibara, T. Goto, K. Yoshimura, and K. Fukamichi, J. Phys.: Condens. Matter **2**, 3381 (1990).

<sup>6</sup>H. Yamada, Phys. Rev. B **47**, 11211 (1993).

<sup>7</sup>R. S. Perry, L. M. Galvin, S. A. Grigera, L. Capogna, A. J. Schofield, A. P. Mackenzie, M. Chiao, S. R. Julian, S. Ikeda, S. Nakatsuji, Y. Maeno, and C. Pfleiderer, Phys. Rev. Lett. **86**, 2661 (2001).

<sup>8</sup>S. A. Grigera, R. P. Perry, A. J. Schofield, M. Chiao, S. R. Julian, G. G. Lonzarich, S. I. Ikeda, Y. Maeno, A. J. Millis, and A. P. Mackenzie, Science **294**, 329 (2001).

<sup>9</sup>C. Pfleiderer, S. R. Julian, and G. G. Lonzarich, Nature (London) **414**, 427 (2001).

<sup>10</sup>S. I. Ikeda, Y. Maeno, S. Nakatsuji, M. Kosaka, and Y. Uwatoko, Phys. Rev. B **62**, R6089 (2000).

<sup>11</sup>B. Binz and M. Sgrist, Europhys. Lett. **65**, 816 (2004).

<sup>12</sup>Y. Maeno, T. M. Rice, and M. Sgrist, Phys. Today **54** (1), 42 (2001).

<sup>13</sup>X. N. Lin, Z. X. Zhou, V. Durairaj, P. Schlottmann, and G. Cao, Phys. Rev. Lett. **95**, 017203 (2005).

<sup>14</sup>G. Cao, L. Balicas, X. N. Lin, S. Chikara, E. Elhami, V. Durairaj, J. W. Brill, R. C. Rai, and J. E. Crow, Phys. Rev. B **69**, 014404 (2004).

<sup>15</sup>G. Cao, L. Balicas, Y. Xin, E. Dagotto, J. E. Crow, C. S. Nelson, and D. F. Agterberg, Phys. Rev. B **67**, 060406(R), (2003).

<sup>16</sup>G. Cao, L. Balicas, Y. Xin, J. E. Crow, and C. S. Nelson, Phys. Rev. B **67**, 184405 (2003).

<sup>17</sup>G. Cao, S. McCall, J. E. Crow, and R. P. Guertin, Phys. Rev. Lett. **78**, 1751 (1997).

<sup>18</sup>G. Cao, K. Abbound, S. McCall, J. E. Crow, and R. P. Guertin, Phys. Rev. B **62**, 998 (2000).

<sup>19</sup>G. Cao, S. McCall, M. Shepard, J. E. Crow, and R. P. Guertin, Phys. Rev. B **56**, R2916 (1997).

<sup>20</sup>G. Cao, S. McCall, M. Shepard, J. E. Crow, and R. P. Guertin, Phys. Rev. B **56**, 321 (1997).

<sup>21</sup>G. Cao, S. McCall, M. Shepard, J. E. Crow, and R. P. Guertin, Phys. Rev. B **56**, R2916 (1997).

<sup>22</sup>C. S. Alexander, G. Cao, V. Dobrosavljevic, S. McCall, J. E. Crow, E. Lochner, and R. P. Guertin, Phys. Rev. B **60**, R8422 (1999).

<sup>23</sup>G. Cao, S. McCall, V. Dobrosavljevic, C. S. Alexander, J. E. Crow, and R. P. Guertin, Phys. Rev. B **61**, R5053 (2000).

<sup>24</sup>G. Cao, S. McCall, J. Bolivar, M. Shepard, F. Freibert, P. Henning, J. E. Crow, and T. Yuen, Phys. Rev. B **54**, 15144 (1996).

<sup>25</sup>M. K. Crawford, R. L. Harlow, W. Marshall, Z. Li, G. Cao, R. L. Lindstrom, Q. Huang, and J. W. Lynn, Phys. Rev. B **65**, 214412 (2002).

<sup>26</sup>G. Cao, L. Balicas, W. H. Song, Y. P. Sun, Y. Xin, V. A. Bondarenko, J. W. Brill, S. Parkin, and X. N. Lin, Phys. Rev. B **68**, 174409 (2003).

<sup>27</sup>X. N. Lin, V. A. Bondarenko, G. Cao, and J. W. Brill, Solid State Commun. **130**, 151 (2004).

<sup>28</sup>R. Gupta, M. Kim, H. Barath, S. L. Cooper, and G. Cao, Phys. Rev. Lett. **96**, 067004 (2006).

<sup>29</sup>Z. Mao, J. Hooper, and D. Fobes, Mater. Res. Bull. **40**, 942 (2005); Z. Mao, J. Hooper, and D. Fobes *et al.*, cond-mat/0406439 (unpublished).

<sup>30</sup>G. Cao, W. H. Song, Y. P. Sun, and X. N. Lin, Solid State Commun. **131**, 331 (2004).

<sup>31</sup>D. J. Singh and I. I. Mazin, Phys. Rev. B **63**, 165101 (2001); I. I. Mazin and D. J. Singh, *ibid.* **56**, 2556 (1997).

<sup>32</sup>The single crystals studied were grown using flux techniques<sup>25</sup> and characterized by single crystal x-ray diffraction at 90 K and room temperature, EDX, and TEM. All results suggest that the crystals studied are of high quality with no impurity or no intergrowth.

<sup>33</sup>T. Valla, P. D. Johnson, Z. Yusof, B. Wellsm, Q. Li, S. M. Loureiro, R. J. Cava, M. Mikami, Y. Mori, M. Yoshimura, and T. Sasaki, Nature (London) **417**, 627 (2002).

<sup>34</sup>A. J. Millis, Phys. Rev. B **48**, 7183 (1993).